Magnesium Technology 2012
Edited by: Suveen N. Mathaudhu, Wim H. Sillekens, Neale R. Neelameggham, and Norbert Hort
TMS (The Minerals, Metals & Materials Society), 2012

Magnesium Technology 2012

Energy and Biomedical / Primary Production

Thursday PM

Session Chair:

Wim Sillekens
(TNO, Netherlands)

Neale Neelameggham
(IND LLC, USA)

Magnesium Technology 2012
Edited by: Suveen N. Mathaudhu, Wim H. Sillekens, Neale R. Neelameggham, and Norbert Hort
TMS (The Minerals, Metals & Materials Society), 2012

IN-VITRO CORROSION STUDIES OF BIOABSORBABLE ALLOYS

P. Gill, N. Munroe
Department of Mechanical and Materials Engineering, Florida International University, Miami, FL, USA

Keywords: magnesium, biodegradable, corrosion, SEM, XRD

Abstract

Magnesium alloys have inspired a significant amount of attention from researchers all over the world for cardiovascular and orthopedic applications due to their light weight, mechanical integrity and degradation behavior. In this investigation, cast manufactured binary, ternary and quaternary magnesium alloys were studied for their degradation behavior by potentiodynamic polarization tests in phosphate buffer saline solution (PBS) and PBS containing amino acids (cysteine, C and tryptophan, W) at 37 °C. Electrochemical impedance spectroscopy (EIS) tests were performed to determine the charge transfer resistance and immersion tests were performed to assess corrosion rate and hydrogen evolution from the alloys. Furthermore, the surface morphology and surface chemistry of the alloys were observed by scanning electron microscopy (SEM) and X-ray diffraction (XRD).

Introduction

Biodegradable alloys are a group of materials, which once implanted, negate further surgical procedures. The demand for better and improved implants has led researchers to explore different types of materials such as: polymers, ceramics, metals and composites. Recently, interest in biodegradable magnesium alloys has increased due to their light weight (low density, close to human bone), mechanical integrity (high strength to weight ratio) and biocompatibility (fourth most abundant cation in human body) [1, 2, 3]. However, these alloys face major challenges with regard to non-uniform corrosion, possibility of premature failure and evolved hydrogen [4]. Alloying is one method of improving the mechanical properties and corrosion resistance of Mg [4]. For bioabsorbable applications, the alloying element must be non-toxic and biocompatible [4, 5], so that the concentration of the dissolved ions once implanted, would not substantially exceed the concentration normally found in human blood [6]. The degradation behavior of magnesium alloys is mainly affected by both intrinsic (composition, microstructure, energy, etc.) and extrinsic factors (temperature, pH, amino acids, chloride ions, etc.) [7].

It has been reported that the corrosion susceptibility of implants may vary with the type of amino acid to which they are exposed [8]. The general structure of amino acids is R–CH(NH_2)–COOH [4, 9], which have a zwitterionic or ampholyte character that is important for the adsorption of molecular species [9]. No significant difference in corrosion susceptibility was observed on exposing Nitinol to amino acids [8]. However, some titanium alloys displayed a slight increase in corrosion susceptibility [9]. There has been little or no significant corrosion studies reported on biodegradable magnesium alloys in amino acids. Chang et al. performed corrosion studies on Mg-Li with amino acids and reported it to have higher corrosion resistance [10]. Yamamoto and Hiromoto studied the effect of amino acids on pure magnesium and reported that amino acids reduced the barrier effect of insoluble salt layer against dissolution of magnesium, which leads to faster dissolution of Mg [11].

In this paper, cast MgZn, MgZnCa and MgZnCaGd alloys were studied for *in-vitro* corrosion properties. Potentiodynamic polarization studies were performed in PBS and PBS containing amino acids, in an attempt to explore their effect on the corrosion behavior of the alloys. Besides, the alloys were also tested for its hydrogen evolution in PBS and surface morphology.

Materials and methods

Cast Mg1Zn, Mg1Zn1Ca and Mg1Zn1Ca1Gd (wt%) alloys were prepared using high purity alloying elements. The alloys were manufactured by melting the elements at 1000 °C under an inert atmosphere (Argon) and casting in a water cooled copper mould. The ramp-up time from room temperature to melting temperature was 1 minute and alloys were further heat treated at 350 °C and water quenched. The ingots were cut into cubes of dimensions 0.414x0.414x0.08 (inch), which were then mechanically polished to achieve a roughness close to 0.05 microns using abrasives and abrasive papers (Buehler) and lubricants (Sigma-Aldrich). Samples were polished in four steps as shown in Table 1. The usage of water based solutions was avoided during sample preparation, in order to prevent the hydrolysis of the alloy. PBS (Sigma Aldrich) and two amino acids (Acros Organics), cysteine (0.25 mM) and tryptophan (0.042 mM) were used as electrolytes for corrosion studies, with the latter at concentrations typically found in human blood [4].

Table 1. Lubricants and abrasives used during sample preparation.

Surface	Lubricant	Abrasive
Carbimet®	Ethanol	SiC, 400 grit
Texmet®	Ethanol-Ethylene Glycol (3:1)	Metadi® Paste, 9 μm
Texmet®	Ethanol-Ethylene Glycol (3:1)	Metadi® Paste, 3 μm
Chemomet®	Ethanol-Ethylene Glycol (3:1)	Masterpolish®, 0.05 μm

Electrochemical testing

A typical three electrode (working, counter and reference) corrosion cell interphased with a potentiostat was used, in which the implant material (working electrode) is placed in deaerated simulated physiological solution, PBS and PBS containing amino acids (PBS+C and PBS+W). The potentiodynamic polarization tests were performed in accordance with ASTM: G 102-89 [12] in PBS (pH = 7.2) at 37 °C employing a GAMRY® potentiostat (G-750). All tests were conducted at a scan rate of 1.0 mV/s. The

electrolyte was purged with high purity nitrogen for 30 minutes prior to immersion of the sample, as well as continuously during the corrosion test. The corrosion rate (CR) of the alloys was determined by:

$$CR = (I_{corr}.K.EW)/(\rho.A)$$

where, I_{corr} is the corrosion current (amps), K is a constant for the corrosion rate (3272 mm/amp.cm.year), EW is the equivalent weight in grams/equivalent, A is the sample area (0.28 cm^2) and ρ is the density (g/cm^3) of the alloys calculated by Archimedes principal (MgZn, 1.75; MgZnCa, 1.76; and MgZnCaGd, 1.85).

Electrochemical impedance spectroscopy (EIS) tests were also performed to determine the effect of alloying elements on the charge transfer resistance at 37 °C in PBS. All tests were conducted in the frequency range from 1.0E-02 Hz to 1.0E+05 Hz with 10 points per decade.

Immersion test

Immersion tests were performed in accordance with ASTM G31-72 [13]. Figure 1 show a schematic representation of the immersion test, where samples were placed at the bottom of a beaker filled with PBS, with a funnel placed above the sample. A solution filled measuring cylinder was placed over the funnel to collect and measure the hydrogen gas evolved as the solution was displaced. The samples were soaked in 300 mL of PBS for 192 hours (9 days) at 37 °C. The hydrogen evolution (per square cm surface area), weight gain and corrosion rate were evaluated during the experiment, by taking the average of three measurements. The samples were weighed before and after 24, 48, 72, 96, 120, 144, 168 and 192 hours. For each time interval, the sample was removed from the PBS, rinsed in distilled water, air dried and then weighed. Once the immersion test was completed, the samples were cleaned by immersing in 180 g/l of chromic acid for 20 min. The weight gain (wt) in grams was calculated as follows [14]:

wt gain = (wt after immersion - wt before immersion)/surface area

The corrosion rates were also calculated from the quantity of hydrogen evolved and weight change during the immersion test. The corrosion rate (CR, mm/year) was calculated as follows:

$$CR = (tW.10)/(\rho AT)$$

where, t is a constant (8760 h), W is mass loss, g (mass before immersion - mass after cleaning)/surface area, A is the surface area before immersion (cm^2), T is the immersion time (h) and ρ is the sample density (g/cm^3).

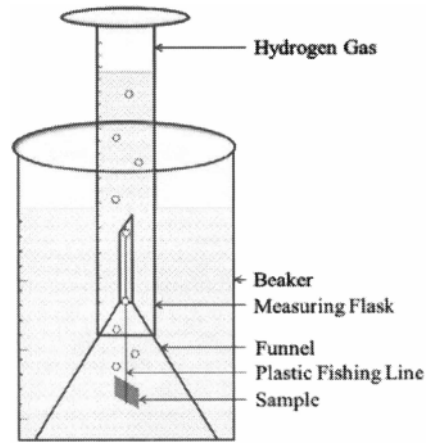

Figure 1. Schematic representation of immersion test setup.

The surface morphology of the mechanically polished alloys before and after corrosion tests was characterized by scanning electron microscopy (SEM, JEOL JSN 6330F). The microstructure phases were determined using XRD (Siemens 5000 D), where Cu-K_α radiation (wavelength, λ = 1.54 A°) operating at 35 mA and 40 kV with a scan rate of 0.01 °/sec over a 2 theta from 20-90° were used.

Results and Discussion

Figure 2 shows the XRD patterns of mechanically polished alloys. The formation of binary phase precipitates was observed in all alloys. The phases: Mg_2Ca, $MgZn_2$, Mg_5Gd [15], were instrumental for precipitation hardening. Zhou et al. reported that MgZnCa alloys synthesized by twin-roll rapid solidification technique produced a large number of precipitates, which contributed to precipitation hardening [16]. Peng et al. manufactured Mg-Gd based alloys and reported superior mechanical properties due to a microstructure composed of fine metastable precipitates dispersed in the matrix [17].

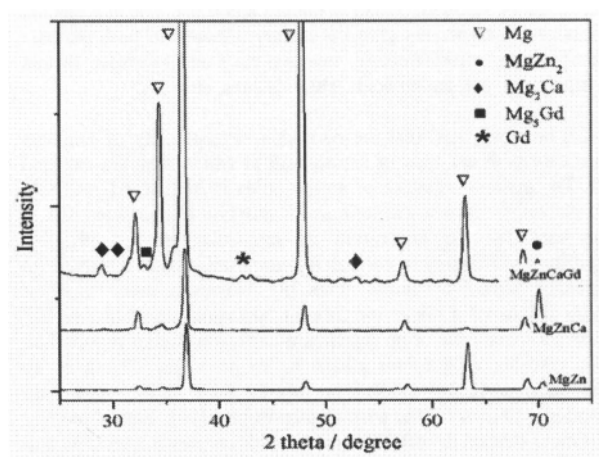

Figure 2. X-ray diffraction pattern of MgZn, MgZnCa and MgZnCaGd.

The morphologies of the alloys before (inset) and after potentiodynamic corrosion tests are compared in Figure 3. Stress induced cracks were observed on the surface of all alloys subjected to potentiodynamic polarization tests in PBS and PBS with amino acids except for MgZn in PBS. MgZnCaGd developed a significant amount of oxides in PBS with cysteine (Figure 2h). Similar cracked corrosion products were reported by various researchers with various Mg alloys [18, 19]. The adsorption of chloride ions on the surface oxides of the alloy lead to the formation of $Mg(OH)_2$ via the hydrolysis of $MgCl_2$ [20]. Dissolution of $MgCl_2$ subsequently exposing the underlying metal surface, which leads to further dissolution of magnesium. At anodic sites, Mg^{++} ions are produced; Cl^- ions diffuse to such sites in order to establish electrical neutrality. $MgCl_2$ is formed in the pits and hydrolyzed according to equation (1) producing hydrochloric acid and further dissolution of Mg.

$$MgCl_2 + 2H_2O \rightarrow Mg(OH)_2 + 2HCl \quad (1)$$

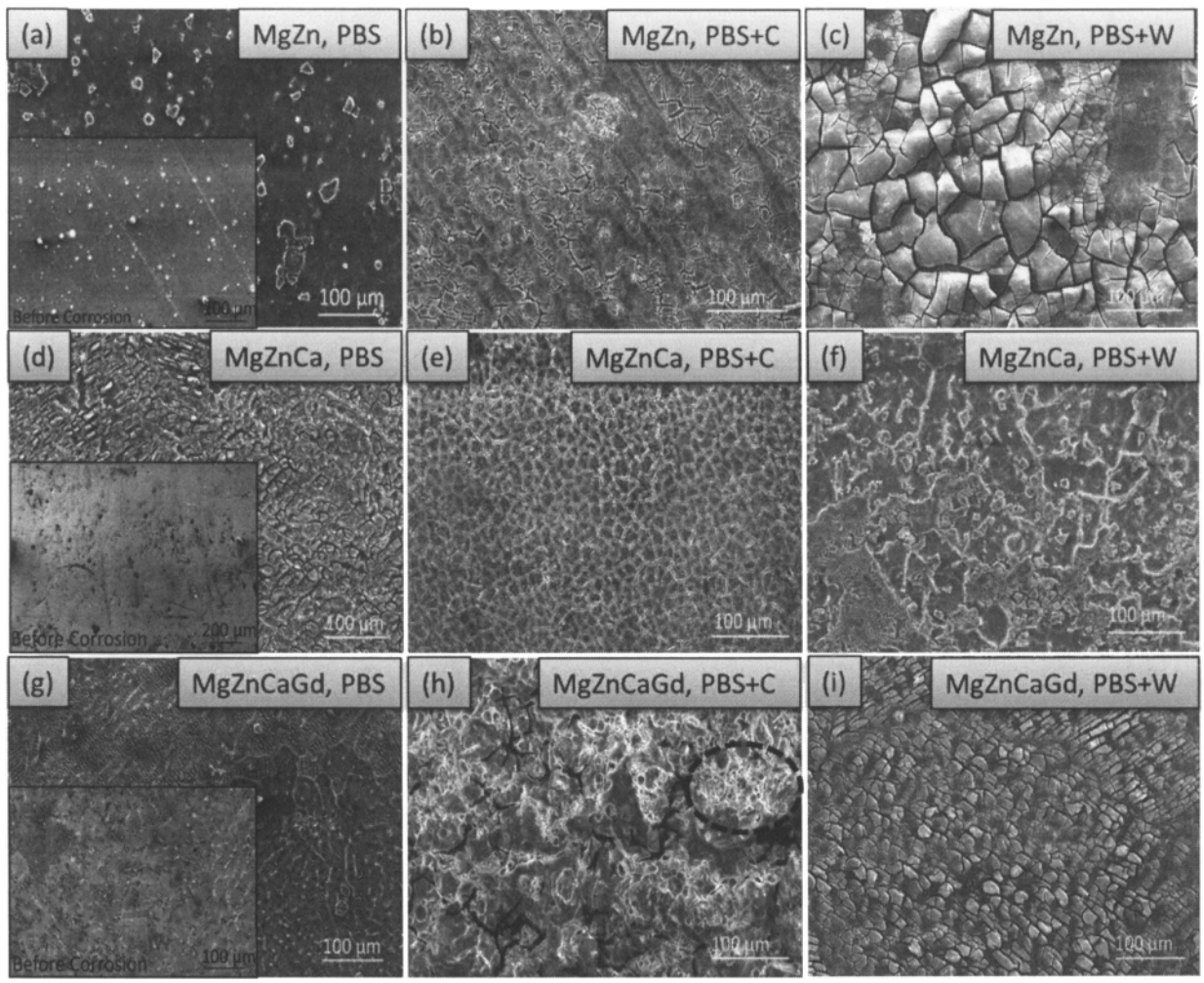

Figure 3. Scanning electron microscopy image of alloys after potentiodynamic corrosion: (a) MgZn, PBS (inset before corrosion); (b) MgZn, PBS+C; (c) MgZn, PBS+W; (d) MgZnCa, PBS (inset before corrosion); (e) MgZnCa, PBS+C; (f) MgZnCa, PBS+W; (g) MgZnCaGd, PBS (inset before corrosion) (h) MgZnCaGd, PBS+C; and (i) MgZnCaGd, PBS+W.

At cathodic sites, water is reduced and hydrogen is evolved in accordance with equation (2).

$$2H_2O + 2e \rightarrow H_2^{\uparrow} + 2OH^- \quad (2)$$

$$Mg + 2H_2O \rightarrow Mg(OH)_2 + H_2 \text{ (overall reaction)} \quad (3)$$

Hydrogen evolution [21] has been reported to result in the formation of gas pockets adjacent to the implant, which delays the healing of tissues and necrosis, equation (3).

Figure 4 (a), shows the volume per unit surface area of hydrogen evolution from the magnesium alloys in PBS at 37 °C over a period of 216 hours. It was observed that the similar volume of

hydrogen was released from all of the alloys during the first 24 hours (Figure 4 (a) inset). After 24 hours, more hydrogen was released from MgZnCaGd, followed by MgZnCa and MgZn. This may be attributed to the formation of four oxides with MgZnCaGd, two of which are those of light metals Mg and Ca (porous oxides of smaller volume) and those of heavy metals, Zn and Gd (non-porous oxides of greater volume) [22]. Mg and Ca oxidize at a rate nearly constant with time (linear equation) whereas, Gd and Zn oxidize proportionally to the logarithm of the time (parabolic equation) [22].

$$y = K_1 t + A_1 \qquad \text{(Linear equation)}$$

$$y_2 = K_2 t + A_2 \qquad \text{(Parabolic equation)}$$

The different oxidation rates of the four oxides induce stresses, which result in the formation of surface cracks seen in the photomicrographs of Figure 3.

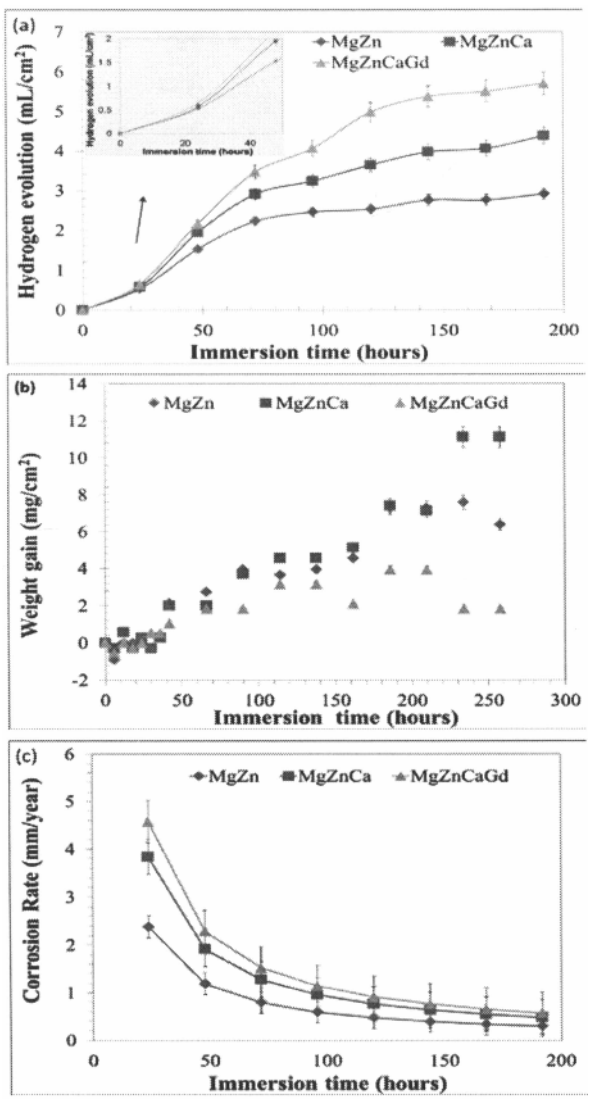

Figure 4. Immersion test of as-cast mechanically polished Mg alloys immersed in PBS for 192 hours at 37 °C: (a) hydrogen evolution volumes; (b) weight gain and (c) corrosion rate.

Figure 4 (b) shows the weight gain of the alloys as function of immersion time. MgZnCa and MgZn exhibited the highest weight gain followed by MgZnCaGd, which may be attributed to the stress induced delamination of the oxide (passivating layer) from the latter, as previously described. The highest weight gain observed in the MgZnCa may be due to the formation three oxides as compared with two for MgZn.

Figure 4 (c) shows the corrosion rate of the alloys as a function of immersion time in PBS at 37 °C. MgZnCaGd exhibited the highest corrosion rate followed by MgZnCa and MgZn. This may be attributed to the relative oxide porosity, cracking and delamination of the oxides in case of the former, which expose the metal to the electrolyte. The rates of corrosion can be inferred from SEM photomicrographs of Figure 4 (c), where there is evidence of uniform corrosion on MgZnCaGd as compared with localized corrosion on MgZn and MgZnCa.

Figure 5 shows the SEM photomicrographs after immersion test for 192 hours in PBS at 37 °C. It was observed that localized corrosion initially occurred at grain boundary sites and then propagated along the grain boundaries (arrows depict pits and circles depict corrosion propagation).

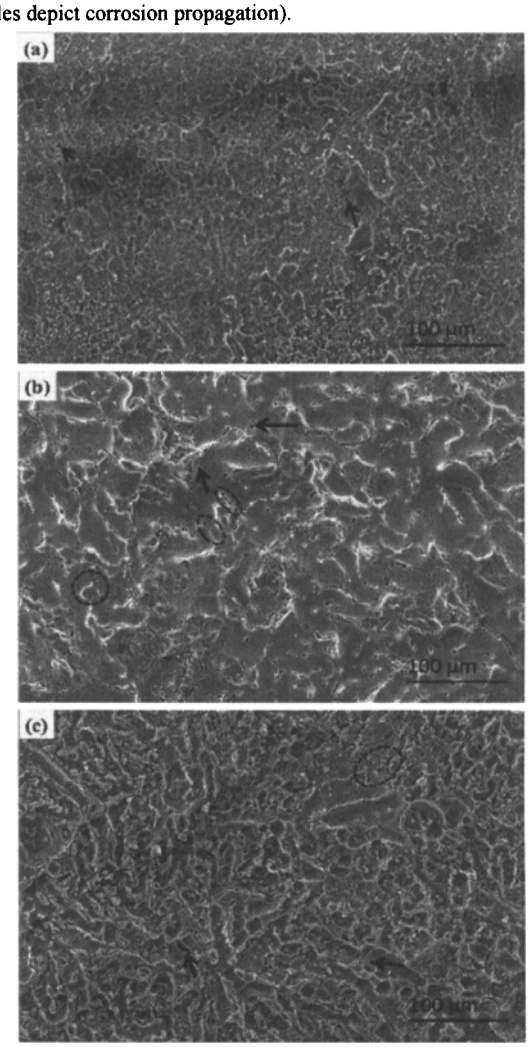

Figure 5. SEM photomicrographs after 192 hours of immersion in PBS: (a) MgZn; (b) MgZnCa and (c) MgZnCaGd.

EDS analysis on the surface of the alloys after immersion for 192 hours are shown in Table 2. The relative concentration of Mg, O, P, K, Zn, Ca and Gd on the surface of the alloys corresponds to the formation of a mixture of apatite, zinc phosphate and calcium phosphate.

Table 2. EDS analysis on the surface of the alloys after immersion in PBS for 192 hours.

Alloys	Element percent, wt%						
	Mg	O	P	K	Zn	Ca	Gd
MgZn	74.0	18.4	4.6	0.2	2.7	-	-
MgZnCa	84.8	10.2	1.7	0.3	2.0	1.1	-
MgZnCaGd	61.1	13.4	3.5	0.5	2.4	0.9	18.2

Figure 6, Nyquist plots revealed an increase in corrosion resistance with the addition of Ca and Gd to MgZn. This could be attributed to the formation of various oxides, which act as an electric barrier. In the case of biodegradable alloys, initial slower corrosion rates followed by uniform degradation are desirable.

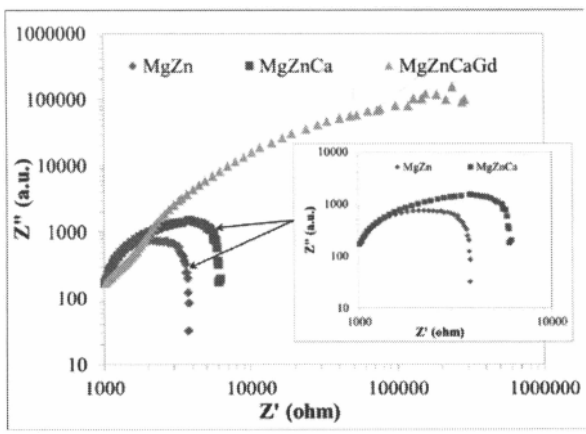

Figure 6. Nyquist plots (log-log representation) for MgZn, MgZnCa and MgZnCaGd in PBS at 37 °C.

Figure 7 shows typical polarization curves for MgZn, MgZnCa and MgZnCaGd alloys, where passivation control occurred between 0.001 - 0.002 A/cm^2. The rough appearance of the anodic curves resulted from continuous breakdown (pitting corrosion) and repassivation [18]. The corrosion parameters of the alloys in PBS and PBS with amino acids are shown in Table 3. MgZn had the lowest corrosion rate in PBS (23.17 mm/year) and exhibited the highest corrosion rate in PBS+W (130.11 mm/year). A similar trend was observed with MgZnCaGd, where the corrosion rate increased in PBS with amino acids. This could be attributed to the acid-base/polarity nature of amino acids. Thus, further studies are required; with titanium alloys, it was reported that amino acids are readily adsorbed onto the surface of TiO_2 via their carboxyl groups by replacing the basic hydroxyl group on a Ti site [9, 23].

MgZn had the highest corrosion potential, E_{corr} (-1.4 V) in PBS, followed by MgZnCaGd (-1.6 V) and MgZnCa (-1.7 V), indicating that MgZn is least susceptible to corrosion followed by MgZnCaGd and MgZnCa.

Table 3. Average potentiodynamic polarization data from three test values in PBS and PBS containing amino acids.

Alloys	E_{corr}, V	I_{corr}, μA	CR, mm/year
MgZn, PBS	-1.4	2.8E-4	23
MgZnCa, PBS	-1.7	6.3E-4	51
MgZnCaGd, PBS	-1.6	5.3E-4	44
MgZn, PBS+C	-1.7	7.9E-4	64
MgZnCa, PBS+C	-1.7	4.7E-4	38
MgZnCaGd, PBS+C	-1.6	19.7E-4	164
MgZn, PBS+W	-1.7	16.0E-4	130
MgZnCa, PBS+W	-1.7	3.5E-4	28
MgZnCaGd, PBS+W	-1.6	18.7E-4	156

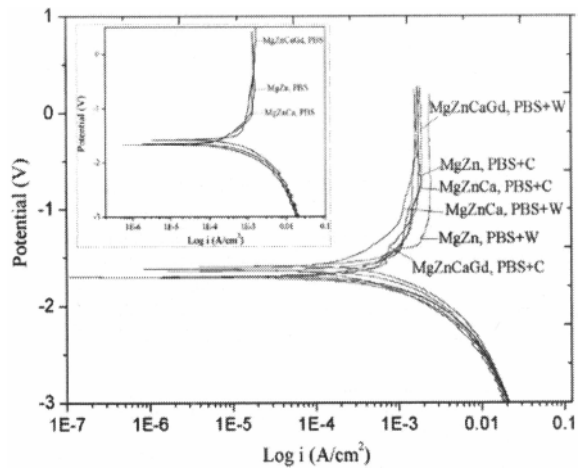

Figure 7. Typical potentiodynamic polarization curves of as-cast magnesium alloys in PBS (inset) and PBS containing amino acids at 37 °C.

Conclusion

XRD depicted the presence of various binary phases, which may improve the mechanical properties of the alloys. Stress induced cracks developed on the surface of all alloys subjected to accelerated corrosion test except for MgZn. Potentiodynamic corrosion tests in PBS revealed that MgZnCa was the most susceptible to corrosion followed by MgZnCaGd and MgZn. In general, the corrosion rates of the magnesium alloys increased when amino acids were added to PBS. Immersion corrosion tests in PBS revealed that MgZnCaGd exhibited the highest corrosion rate followed by MgZnCa and MgZn. However, it should be noted that there was no significant difference in the corrosion rates of MgZnCa and MgZnCaGd in PBS for either accelerated or immersion corrosion tests. Photomicrographs of alloys immersed in PBS revealed that localized corrosion initially occurred at grain boundary sites, then, propagated along the grain boundaries. Nyquist plots depicted an increase in corrosion resistance with the addition of alloying elements, due to the formation of various oxides.

Acknowledgement

P.G. and N.M. acknowledge Dr. H. T. Lin and Amit Datye from Oak Ridge National Laboratory (ORNL) for their helpful discussions. P.G. acknowledges the Dissertation Evidence Acquisition Fellowship from University Graduate School Florida International University.

N.M. would like to acknowledge the financial support from National Institute of General Medical Sciences Award Number SC3GM084816.

References

1. R.K. Rude, "Magnesium deficiency: A cause of heterogeneous disease in humans", J Bone Miner Res, 13 (1998), 749-58.
2. M.E. Shils, Magnesium. In: Shils ME, Olson JA, Shike M, editors (Modern nutrition in health and disease, 8th ed. Philadelphia: Lea & Febiger (1994), 164–84.
3. G.L. Song, A. Atrens, "Corrosion mechanisms of magnesium alloys", Advanced Engineering Materials, 1 (1999), 11-33.
4. M.P. Staiger, A.M. Pietak, J. Huadmai, G. Dias, "Magnesium and its alloys as orthopedic biomaterials: A review", Biomaterials, 27 (2006), 1728–1734.
5. B. Heublein, R. Rohde, V. Kaese, M. Niemeyer, W. Hartung, A. Haverich, "Biocorrosion of magnesium alloys: a new principle in cardiovascular implant technology?", Heart, 89 (2003), 651–656.
6. H.X. Wang, S.K. Guan, X. Wang, C.X. Ren, L.G. Wang, "In vitro degradation and mechanical integrity of Mg–Zn–Ca alloy coated with Ca-deficient hydroxyapatite by the pulse electrodeposition process", Acta Biomaterialia, 6 (2010), 1743–1748.
7. W. Haider, "Enhanced Biocompatibility of NiTi (NITINOL) Via Surface Treatment and Alloying" Ph.D. thesis, Florida International University (2010), 177.
8. B.G. Pound, "Corrosion behavior of nitinol in blood serum and PBS containing amino acids", J Biomed Mater Res B Appl Biomater, 2 (2010), 287-295.
9. P. Gill, N. Munroe, C. Pulletikurthi, S. Pandya, W. Haider, "Effect of Manufacturing Process on the Biocompatibility and Mechanical Properties of Ti-30Ta Alloy", J Mater Eng Perform, 20 (2011), 819-823.
10. L. Chang, P. Wang, W. Liu, "Effect of amino acids on the structure and corrosion resistance of Mg-Li alloy anodic oxide film", Advanced Materials Research, 146-147 (2010), 785-788.
11. A. Yamamoto, S. Hiromoto, "Effect of inorganic salts, amino acids and proteins on the degradation of pure magnesium in vitro", Materials Science and Engineering C, 29 (2009), 1559–1568.
12. ASTM G102-89 (1999), Standard Practice for Calculation of Corrosion Rates and Related Information from Electrochemical Measurements. DOI: 10.1520/G0102-89R99.
13. ASTM G31-72 (2004), Standard Practice for Laboratory Immersion Corrosion Testing of Metals. DOI: 10.1520/G0031-72R04.
14. L. Xu, E. Zhang, D. Yin, S. Zeng, K. Yang, "In vitro corrosion behaviour of Mg alloys in a phosphate buffered solution for bone implant application", J Mater Sci: Mater Med, 19 (2008), 1017-1025.
15. Z. Li, X. Gu, S. Lou, Y. Zheng, "The development of binary Mg–Ca alloys for use as biodegradable materials within bone", Biomaterials, 29 (2008), 1329–1344.
16. T. Zhou, D. Chen, Z. Chen, "Microstructures and properties of rapidly solidified Mg-Zn-Ca alloys", Trans. Nonferrous Met. Soc. China, 18 (2008), 101-106.
17. Q. Peng, X. Hou, L. Wang, Y. Wu, Z. Cao, L. Wang, "Microstructure and mechanical properties of high performance Mg–Gd based alloys", Materials and Design, 30 (2009), 292–296.
18. Y. Wang, C.S. Lim, C.V. Lim, M.S. Yong, E.K. Teo, L.N. Moh, "In vitro degradation behavior of M1A magnesium alloy in protein-containing simulated body fluid", Materials Science Engineering C, 31 (2011), 579-587.
19. Y. Song, D. Shan, R. Chen, F. Zhang, E.H. Han, "Biodegradable behaviors of AZ31 magnesium alloy in simulated body fluid", Materials Science and Engineering C, 29 (2009), 1039–1045.
20. R. Ambat, N.N. Aung, W. Zhou, "Studies on the influence of chloride ion and pH on the corrosion and electrochemical behaviour of AZ91D magnesium alloy", Journal Applied Electrochemistry, 30 (2000), 865-874.
21. G. Song, "Control of biodegradation of biocompatable magnesium alloys", Corrosion Science, 49 (2007), 1696-1701.
22. H.H. Uhlig, The corrosion handbook (John Wiley & Sons, Inc. (1948), 15.
23. M. Schmidt, S.G. Steinemann, "XPS studies of amino acids adsorbed on titanium dioxide surfaces", J. Anal. Chem, 314 (1991), 412–415.